ELSEVIER

Journal of Alloys and Compounds 223 (1995) 130–138

Journal of ALLOYS AND COMPOUNDS

Comparative study of some rare earth sulfides: doped γ-[A]M_2S_3 (M = La, Ce and Nd, A = Na, K and Ca) and undoped γ-M_2S_3 (M = La, Ce and Nd)

R. Mauricot, P. Gressier, M. Evain, R. Brec *

Laboratoire de Chimie des Solides, IMN, UMR CNRS No. 110, Université de Nantes, 2 rue de la Houssinière, 44072 Nantes Cedex 03, France

Received 11 October 1994; in final form 7 November 1994

Abstract

The crystal structure determination of γ-M_2S_3 compounds (M = La, Ce, and Nd) has been carried out for the first time from single crystals obtained through high-temperature melting under sulfur pressure. The three phase structures do not depart from the cubic Th_3P_4 structural type, with a statistical filling of the dodecahedral sites by the cations. The γ-$Na_{0.5}Ce_{2.5}S_4$-doped phase structure has also been determined from a powder neutron diffraction study. Na^+ was found to be located at the dodecahedral site, in agreement with the composition limit of Na/Ce = 0.20 as determined by cell parameter variation versus composition. A powder X-ray diffraction study of the potassium- and calcium-doped derivatives (γ-$K_{0.46}C_{2.54}S_4$ and γ-$Ca_{0.89}Ce_{2.07}S_4$) confirmed the results obtained for the sodium-doped phase. In no case, at least in the phases studied, does the alkali or alkaline earth metal occupy the inter-dodecahedral tetrahedral sites. The electronic band structures of Ce_2S_3 and of $Ce_{3-x}S_4$ ($0 < x < 1/3$) indicate an insulating behavior for the former compound and a metallic behavior for the latter, assuming in this case a rigid band model. In Ce_3S_4, the electronic conductivity takes place along the Ce–Ce bonds. No S–S bonding was found in the two binaries. It seems possible to assign the color of some γ-M_2S_3 materials to electronic transitions to the conduction band from (i) the valence band (La_2S_3), (ii) the 4f level (Ce_2S_3) and (iii) the 4f and valence band (Nd_2S_3).

Keywords: Sodium; Potassium; Calcium; Electronic transition versus colour

1. Introduction

The impact of legislation on limiting the use of some pigments has given an impetus to the search for new inorganic, non-toxic pigments, particularly in the yellow to red color range. Indeed, very few red inorganic pigments are available for the plastics industry. Essentially cadmium sulfoselenide, lead molybdate and iron(III) oxide are known. The first compound meets the required criteria best, but international regulations tend to exclude it, because pyrolysis of cadmium-containing materials results in the emission of cadmium oxide, which is dangerous for public health and the environment. The other two phases are orange and dark red, respectively. Thus, today, the sole use of high-performance, organic red pigments is considered. However, these pigments have strong limitations such as a very high cost (up to ten times the inorganic compound prices) and thermal and UV instability.

The use of cerium sulfide-based pigments, which fulfil preparation, color and stability requirements, has been explored [1]. In order to control color shades, it is necessary to know precisely the origin of the electronic transitions which are responsible for the observed colors. This is the reason why structural determination and band structure calculations were performed on some doped [A_x]M_2S_3 (M = La, Ce and Nd; A = Na, Ca, and K) or undoped M_2S_3 (M = La, Ce, and Nd) rare earth sulfides, in their high-temperature γ-phase. Lanthanum and neodymium phases were studied to facilitate the understanding of the cerium phase, which they flank.

2. Experimental

Rare earth sulfides can be obtained either as powders or in monocrystalline form, depending on the synthesis conditions. Our samples were synthesized by circulating H_2S over a cerium derivative at high temperature (700–1300 °C) for more than 4 h. Alkaline or alkaline

* Corresponding author.

SSDI 0925-8388(94)01476-O

earth doping was performed during synthesis. A full elemental analysis was completed on the various samples. La_2S_3, Ce_2S_3 and Nd_2S_3 monocrystals were provided by the Inorganic Chemistry Institute of Novosibirk (Russia). Their preparation is fully described in Ref. [2]. Basically, these crystals were extracted from a rare earth sulfide melt, obtained in a quartz device heated beyond the melting point of the target compound in an HF furnace. Their sizes were several millimeters in all three directions. Tiny fragments were cut out for X-ray studies.

Powder X-ray diffraction patterns were collected on a Siemens D5000 diffractometer with an incident-beam monochromator ($\lambda = 1.540\,598$ Å). A 0.03° step scanning was used in the 20–140° (2θ) range. The pattern analysis and the lattice parameters were performed with the U-FIT [3] and PROLIX [4] programs, respectively; the structure refinements were conducted with the FULLPROF [5] code. Owing to too large a difference between scattering factors of rare earth and alkaline metal atoms, the study of γ-$[Na_x]Ce_2S_3$ was performed using neutron diffraction at the Laboratoire Léon Brillouin at Saclay (France), with the following data conditions: monochromatized incident beam ($\lambda = 1.98450$ Å) and step scanning (0.05°) in the 1–149° (2θ) range.

γ-La_2S_3, γ-Ce_2S_3, and γ-Nd_2S_3 monocrystal studies were made using a four-circle Siemens (P4) diffractometer. Structures were refined by means of MOLEN [6], XTAL [7] and SHELXTL [8] codes. For each phase, reflection data were collected in a half sphere, to check for possible departure from cubic symmetry. The γ-Ce_2S_3 crystal shape was parallelepipedic, and thus face indexing was successful, allowing for absorption corrections by gaussian integration. The γ-La_2S_3 and γ-Nd_2S_3 crystal shapes being irregular, semi-empirical absorption corrections were performed from a Psi dependence analysis (see Table 1 for data collection conditions and refinement critiria).

Electronic band structures were calculated using the semi-empirical extended Hückel method [9].

3. Monocrystal studies

3.1. γ-Ce_2S_3 structure determination

Many years ago, Zachariasen [10] showed from X-ray diffraction powder patterns that the γ-phase of M_2S_3 rare earth sulfides crystallizes with cubic symmetry in the $I\bar{4}3d$ space group and is isotypic with Th_3P_4. Indeed, this structure can be considered as deriving from the Th_3P_4 framework by partial removal of the cations yielding the lacunar formulation $Ce_{8/3}\square_{1/3}S_4$, in agreement with an oxidation state of III for cerium and a semiconducting behavior of the phase. Furthermore, Ce_3S_4 also exists with a purely Th_3P_4-type structure and a metallic behavior [11]. A first refinement attempt on the γ-Ce_2S_3 structure from the diffraction powder pattern confirmed the structural type, but seemed to show a slight distortion, some line intensities not being well calculated. This structural disagreement could be attributed to an ordering of the vacancies in the γ-

Table 1
Crystallographic data for some γ-M_2S_3 phases and data collection conditions

Formula	$La_{2.666}S_4$	$Ce_{2.666}S_4$	$Nd_{2.666}S_4$
Molecular weight (g)	498.67	501.90	512.90
Space group	$I\bar{4}3d$	$I\bar{4}3d$	$I\bar{4}3d$
a (Å)	8.731(2)	8.651(2)	8.529(2)
V (Å^3)	665.5(4)	647.4(4)	620.4(4)
Z	4	4	4
ρ (g cm^{-3})	4.98	5.15	5.49
Radiation	Mo K–$L_{2,3}$	Mo K–$L_{2,3}$	Mo K–$L_{2,3}$
Crystal size (mm)	Fragment	0.0254×0.0429×0.0175	Fragment
μ (cm^{-1})	179.5	196.0	232.1
Scan mode	$\omega/(2\theta)$	$\omega/(2\theta)$	$\omega/(2\theta)$
Recording range (θ)	2.0–80.0°	2.0–80.0°	2.0–80.0°
Standard reflections	310, 132, 2–13	310, 132, 2–13	310, 132, 2–13
hkl Domains	$-15<h<15$ $-15<k<15$ $-15<l<15$	$-15<h<15$ $-15<k<15$ $-15<l<15$	$-15<h<15$ $-15<k<15$ $-15<l<15$
Recorded reflections	5106	4500	4300
Independent reflections with $I>2.5\sigma(I)$	321	283	331
R_{int}	0.042	0.041	0.075
R	0.020	0.028	0.038
R_w	0.025	0.029	0.042

Ce_2S_3 structure, as suggested earlier by Carter [12], although no satellite reflections could be observed. Therefore, a single-crystal structure determination of γ-Ce_2S_3 was initiated.

The refinement in the $I\bar{4}3d$ space group converged quickly, with cerium and sulfur on positions 12a and 16c, respectively. The cationic site occupation was then refined and, taking into account the anisotropic atomic displacement parameters (ADPs), the reliability factor R converged to a final value of 2.8% ($R_w = 2.9\%$). The very good value of the refinement factors and the absence of difference Fourier residues proved the assigned structural framework and symmetry to be correct. The internal reliability factor ($R_i = 4.1\%$) on averaging equivalent reflections in the Laue group was also further good evidence for this conclusion. The unsatisfactory refinement of the powder pattern must therefore be attributed to some preferred orientation problems. Complementary powder diffraction studies with an INEL diffractometer working in the Debye–Scherrer mode, a set-up less prone to such orientation, confirmed this hypothesis. In Table 2 are gathered the results of the powder pattern parameter refinement while Table 1 presents the single crystal refinement results. Table 3 gives atomic position parameters together with anisotropic ADPs.

3.2. γ-La_2S_3 and γ-Nd_2S_3 structure determination

The powder diagram profile and cell parameter refinement for both phases being satisfactory, it was certain that their structure was derived directly from the Th_3P_4 structure type. Structure refinements were then completed as with the cerium compound, i.e. from single-crystal data. They confirmed the structural type. Reliability factors converged to $R = 2.0\%$ ($R_w = 2.5\%$) and $R = 3.8\%$ ($R_w = 4.2\%$) for La_2S_3 and Nd_2S_3, respectively. The latter refinement factor is higher than the former, probably owing to a poorer crystal quality and/or a less accurate absorption correction. Nevertheless, in case of possible distortion, although no anomaly was detected on the powder diffraction pattern of this phase, a refinement was carried out in a rhombohedral subgroup $R3c$, after averaging of the equivalent reflections in this new group. The best results were worse than in the cubic symmetry, with $R = 5.8\%$ and $R_w = 6.9\%$. The occurrence of an inferior symmetry in the M_2S_3 series is to be definitively rejected. Table 1 presents the complete single-crystal refinement results on γ-La_2S_3 and γ-Nd_2S_3, while Table 3 gives the atomic positions and the anisotropic ADPs. The M–S and S–S main distances are given in Table 4.

These three studies together confirm that γ-M_2S_3 phases (M = La, Ce and Nd) are cubic with space group $I\bar{4}3d$, and that cations are randomly distributed in the metal sub-lattice.

Table 2
Parametric data for γ-Ce_2S_3 powder diagram ($a = 8.6350(2)$ Å).

h k l	d_{cal}	d_{obs}	I_{obs}
2 1 1	3.525	3.525	84
2 2 0	3.0530	3.0538	5
3 1 0	2.7306	2.7312	100
3 2 1	2.3078	2.3073	51
4 0 0	2.1588	2.1589	5
4 2 0	1.9310	1.9313	52
3 3 2	1.8410	1.8410	14
4 2 2	1.76263	1.76266	8
4 3 1 5 1 0	1.69348	1.69356	20
5 2 1	1.57654	1.57604	6
4 4 0	1.52648	1.52633	2
5 3 2 6 1 1	1.40080	1.40073	25
6 2 0	1.36533	1.36532	6
5 4 1	1.33242	1.33247	10
6 3 1	1.27317	1.27323	3
4 4 4	1.24637	1.24647	19
6 4 0	1.19747	1.19747	9
5 5 2 6 3 3	1.17509	1.17512	30
6 4 2	1.15391	1.15396	4
7 3 2 6 5 1	1.09660	1.09654	6
6 5 3	1.03209	1.03213	7
7 4 3 8 3 1 7 5 0	1.00381	1.00375	27
7 5 2	0.97773	0.97765	2
8 4 0	0.96543	0.96540	9
8 4 2	0.94216	0.94220	9
6 5 5 7 6 1 9 2 1	0.93114	0.93115	16
7 5 4 8 5 1 9 3 0	0.91022	0.91021	27
9 3 2	0.89064	0.89062	5
8 4 4	0.88131	0.88134	3
10 1 1	0.85500	0.85499	9
8 6 2	0.84674	0.84671	3
9 4 3	0.83871	0.83868	17

3.3. γ-M_2S_3 structure description

Although Th_3P_4 type is well known, a brief description may be useful, because some doped phases were obtained with the same structural model (see below). Each metal atom is surrounded by eight sulfur atoms building a regular triangular dodecahedron. Each dodecahedron shares with its neighbors either one triangular face or one edge (Figs. 1 and 2, respectively). Between two neighboring dodecahedra sharing one

Table 3
Atomic positions and displacement parameters of γ-Ce_2S_3, γ-La_2S_3 and γ-Nd_2S_3

Atom	x	y	z	B_{eq} [a]	$\tau_{occupation}$	
Ce	3/8	0	1/4	1.08(3)	0.888	
S	0.0731(2)	0.0731	0.0731	0.058(5)	1	
La	3/8	0	1/4	1.232(3)	0.869(5)	
S	0.0734(2)	0.0734	0.0734	1.266(5)	1	
Nd	3/8	0	1/4	1.02(1)	0.885(3)	
S	0.0721(2)	0.0721	0.0721	1.01(6)	1	
	U_{11} [b]	U_{22}	U_{33}	U_{12}	U_{13}	U_{23}
Ce	1.48(5)	1.31(3)	1.31	0	0	0
S	1.41(6)	1.41	1.41	0.07(6)	0.07	0.07
La	1.66(3)	1.57(2)	1.57	0	0	0
S	1.38(5)	1.38	1.38	0.05(5)	0.05(5)	0.05
Nd	1.43(3)	1.23(3)	1.23	0	0	0
S	1.28(8)	1.28(8)	1.28	0.09(5)	0.09	0.09(5)

[a] Isotropic equivalent ADP defined as

$$B_{eq}\,(\text{Å}) = \frac{4}{3}\,\text{trace}(\beta\mathbf{g}) \text{ or } B_{eq} = \frac{8\pi^2}{3}\sum_i\sum_j U_{ik}\,|\mathbf{a}_i^*||\mathbf{a}_j^*|\,|\mathbf{a}_i\cdot\mathbf{a}_j.$$

The expression of the harmonic displacement factor is

$$\exp\left(-2\pi^2\sum_i\sum_j U_{ij}\,|\mathbf{a}_i^*||\mathbf{a}_j^*|\,h_ih_j\right), \text{ with } U_{ij} \text{ in Å}^2.$$

[b] $100\times U_{ij}$ (Å^2).

Table 4
Main interatomic distances (Å) in the three γ-M_2S_3 phases (M = La, Ce and Nd)

Distance	La_2S_3	Ce_2S_3	Nd_2S_3
M–M	4.0836(5) (×8)	4.0461(5) (×8)	3.9891(5) (×8)
	4.8808(7) (×4)	4.8361(7) (×4)	4.7679(7) (×4)
	5.9777(9) (×8)	5.9229(9) (×8)	5.8394(9) (×8)
M–S	2.932(1) (×4)	2.901(2) (×4)	2.851(1) (×4)
	3.116(1) (×4)	3.092(2) (×4)	3.058(1) (×4)
S–S	3.338(2) (×3)	3.312(2) (×3)	3.274(2) (×3)
	3.780(2) (×3)	3.746(2) (×3)	3.693(2) (×3)
	4.194(2) (×6)	4.151(2) (×6)	4.082(2) (×6)

edge, a very distorted empty S_4 tetrahedron can be observed. Its center sits at the Wyckoff position 12c. This is, with the center of the dodecahedra not fully occupied by a rare earth atom, the second remarkable site of the structure. Both types of voids are potential host sites for Na-, K- or Ca-doped phases. Their recognition is then important for the pursuit of the study.

4. Study of γ-$Na_{0.5}Ce_{2.5}S_4$

The influence of an alkali metal may be manifested in the color modification it induces in the host material.

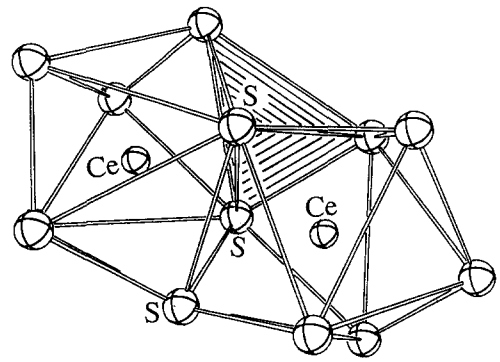

Fig. 1. Two MS_8 dodecahedra sharing one triangular face in the γ-M_2S_3 phases. Note the presence of an empty (hatched) S_4 tetrahedron between two dodecahedra.

In the case of sodium, a thorough X-ray diffraction study of the a cubic parameter as a function of the ratio y = Na/Ce shows a linear variation for y ranging from 0 to 0.20, in agreement with a monophasic domain (see Fig. 3). Beyond $x = 0.20$, the a parameter is constant, while a rock-salt type phase, $NaCeS_2$, appears. From this, it follows clearly that, if a hypothesis of a substitution of sodium for cerium is made, the monophasic domain limit is due to structural factors. Moreover, the precise limit of $y = 0.20$ implies a maximum composition with the formula $Na_{0.5}Ce_{2.5}S_4$. This would then

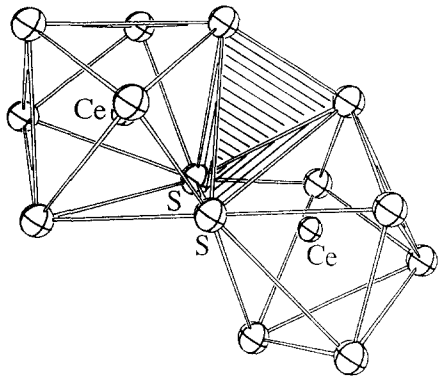

Fig. 2. Two MS_8 dodecahedra sharing one edge in the γ-M_2S_3 phases. Note the presence of an empty (hatched) S_4 tetrahedron between two dodecahedra.

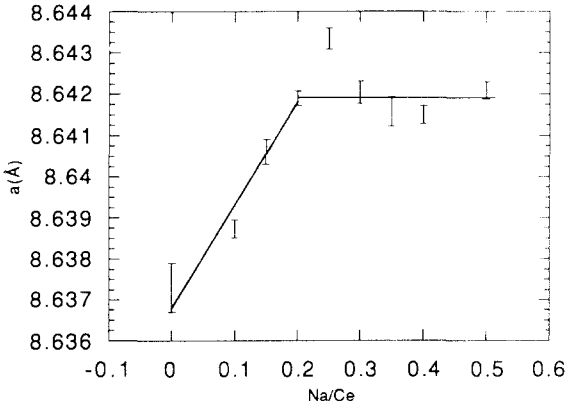

Fig. 3. Cell parameter variation as a function of y = Na/Ce ratio for γ-$Ce_{2.667-x}Na_{3x}S_4$.

correspond to a total filling of the dodecahedral sites. In order to confirm this distribution, and to rule out the possible occupation of the available tetrahedral sites of the structure, a powder neutron diffraction study was undertaken. A nominal composition richer than the maximum composition of the monophasic domain was chosen to ensure a maximum concentration of sodium ions, hence a most precise analysis. A structural determination with the Rietveld method [5] enabled us to establish that there is no sodium in the tetrahedral sites, and that all the sodium ions sit with the cerium ions in the dodecahedral sites. The refinements converged to a value of $R_p = 5.63\%$ ($R_{wp} = 4.40\%$ and $R_{Bragg} = 1.69\%$) (Fig. 4). The sum of the occupation ratio of the cerium and sodium sites was constrained to 1.0. $\tau_{Na} = 16\%$ and $\tau_{Ce} = 84\%$ values were obtained, in a good agreement with the limit of composition Na/Ce = 0.20. However very large standard deviations occurred (related to high correlation coefficients), which forced us to fix the ratio at the theoretical values without refining them. The solid solution formulation can clearly be written as $Ce_{2.667-x}Na_{3x}S_4$ ($0 \le x \le 1/6$). Additionally, the parasitic phase $NaCeS_2$ was simultaneously refined in the NaCl structural type

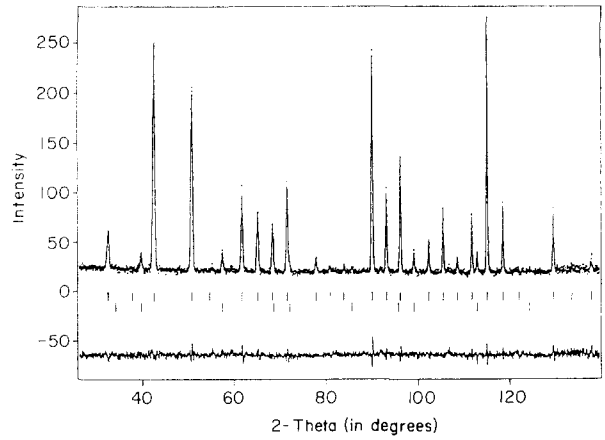

Fig. 4. Neutron diffraction Rietveld refinement results of the γ-$Na_{0.5}Ce_{2.5}S_4$ and $NaCeS_2$ phase mixing.

($R_{Bragg} = 13.1\%$ for $NaCeS_2$). All refinement results are reported on Table 5. Note that atomic positions are very near to those of the undoped phase.

5. Study of γ-$K_{0.46}Ce_{2.54}S_4$

The preceding results were confirmed by doping with a heavier alkali metal, e.g. potassium. Owing to the much higher atomic number of K, X-ray diffraction pattern refinement could be completed. In Table 6, all parameters of the structural refinements on the phase $K_{0.46}Ce_{2.54}S_4$ are gathered. During Rietveld calculations, the occupation ratio of potassium on tetrahedral site converged to zero, while the R_p factor value reached 11.3% ($R_{wp} = 12.3\%$) with potassium and cerium sitting on the same position ($R_{Bragg} = 9.1\%$).

6. Study of γ-$Ca_{0.89}Ce_{2.07}S_4$

With the calcium-doped compound, we definitely demonstrated that an insertion of alkali or alkaline earth metal ions on empty dodecahedral sites occurs together with a substitution of cerium ions by alkali or alkaline earth metal ions. In the case of a reaction with a 2+ ion, the general formulation $Ce_{2.667-x}Ca_{1.5x}S_4$ ($0 \le x \le 2/3$) is expected. A compound with Ca/Ce = 0.43, near the expected limit of $CaCe_2S_4$, i.e. Ca/Ce = 0.50, was obtained. Owing to the high scattering factor of the calcium atom, structural determination by the Rietveld method could be achieved from an X-ray diffraction pattern. Refinement converged to $R_p = 15.1\%$ ($R_{wp} = 17.1\%$) and showed again an insertion/substitution only on dodecahedral sites. Calculations were carried out with fixed B_{iso} values because of their divergence after some cycles owing to strong correlation with the occupation ratio. Fixed values were those reached in the first cycles. Fig. 5 and Table 7 show

Table 5
Structure refinement results for the neutron diffraction diagram of a $Na_{0.5}Ce_{2.5}S_4$ and $NaCeS_2$ mixing with nominal ratio Na/Ce = 0.30

Phase	Atoms	x	y	z	B_{iso} (Å^2)	$\tau_{occupation}$
$Na_{0.5}Ce_{2.5}S_4$ (a = 8.6371(1) Å)	Ce	3/8	0	1/4	0.87(5)	5/6
	Na	3/8	0	1/4	0.87	1/6
	S	0.0725(2)	0.0725	0.0725	0.73(7)	1
$NaCeS_2$ (a = 5.8286(2) Å)	Ce	0	0	0	0.87(5)	1/2
	Na	0	0	0	0.87	1/2
	S	1/2	1/2	1/2	0.73(7)	1

Table 6
Structure refinement results for the X-ray diffraction diagram of the $K_{0.46}Ce_{2.54}S_4$ phase (a = 8.6834(1) Å)

Atom	x	y	z	B_{eq} (Å^2)	$\tau_{occupation}$
Ce	3/8	0	1/4	0.41(5)	0.85(2)
K	3/8	0	1/4	0.41	0.15
S	0.0713(6)	0.0713	0.0713	0.41(7)	1

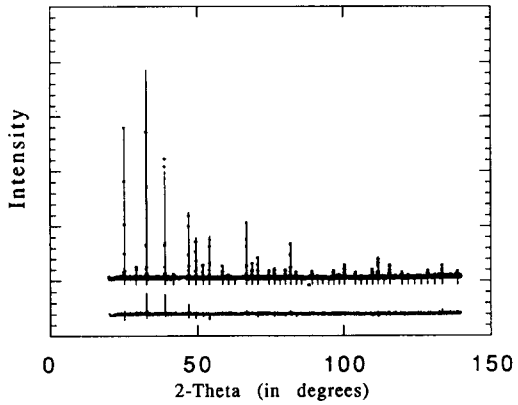

Fig. 5. Rietveld refinement results of the γ-$Ca_{0.89}Ce_{2.07}S_4$ X-ray powder diffraction pattern.

Table 7
Structure refinement results for the X-ray diffraction diagram of the $Ca_{0.89}Ce_{2.07}S_4$ phase

Atom	x	y	z	B_{iso} (Å^2)	$\tau_{occupation}$
Ce	3/8	0	1/4	0.43	0.69(6)
Ca	3/8	0	1/4	0.43	0.29(6)
S	0.0724(7)	0.0724	0.0724	0.34	1

the observed, calculated and difference diagrams and the refinement parameters, respectively. These calculations with constrained isotropic ADPs are in excellent agreement with the above general formulation.

7. Electronic structure of cerium sulfides

7.1. Stoichiometric Ce_3S_4

To obtain the band structure of a solid in reciprocal space, this solid has to be a periodic one. That is why we began this study with stoichiometric Ce_3S_4, planning to use the results for lacunar Ce_2S_3 in a rigid band scheme. Semi-empirical parameters used in the calculation are given in Table 8.

Table 8
Semi-empirical parameters used in the band structure calculation of γ-Ce_3S_4 with the extended Hückel method [9]

AO	3s (S)	3p (S)	6s (Ce)	6p (Ce)	5d (Ce)[a]
H_{ii} (eV)	−20.00	−13.30	−7.67	−5.01	−10.21
Slater exponents ζ_i	1.817	1.817	2.14	2.08	3.78 (0.776 51) 1.381 (0.458 61)

[a] Two exponents are given for the 5d atomic orbitals. Each is followed, in parentheses, by its coefficient in the expression in double ζ.

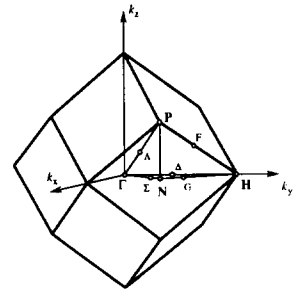

Fig. 6. Band structure near the Fermi level e_f of γ-Ce_3S_4 along high-symmetry lines of the zone drawn in Fig. 7.

Very localized cerium 4f atomic orbitals (AO) are not taken into account: we consider that the 4f cerium electron, whose existence is revealed by the magnetic behavior of the phase [13], does not take part in the formation of bands, but sits on a level at a well defined energy.

Fig. 6 shows the band structure near the Fermi level e_f of Ce_3S_4 along high-symmetry lines of the $Ce_{12}S_{16}$ cubic cell first Brillouin zone (drawn in Fig. 7). The bands that cross the Fermi level have a great dispersion along different reciprocal space directions. This agrees with a good isotropic metallic behavior of Ce_3S_4 [14].

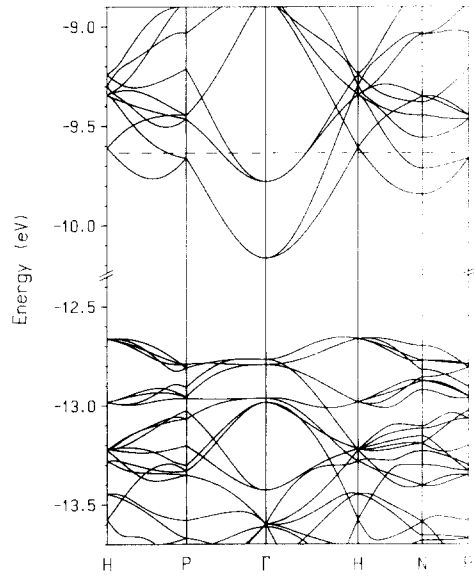

Fig. 7. First Brillouin zone of $Ce_{12}S_{16}$ cubic cell.

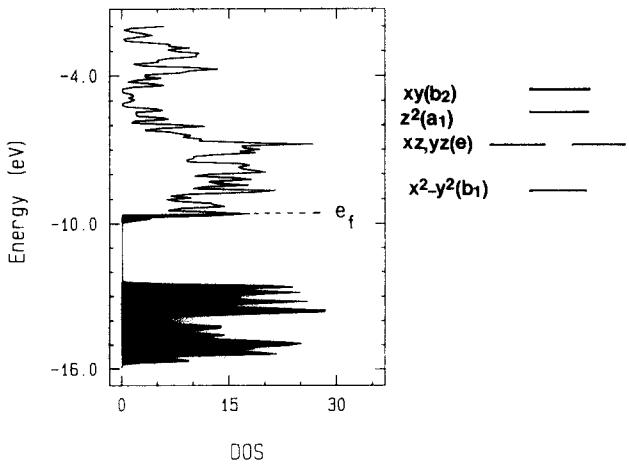

Fig. 8. Density of states (electrons per eV per Ce_6S_8 unit cell) of Ce_3S_4 (left) and energy d levels of CeS_8 dodecahedron (right). Overlap integrals computed up to a 7 Å distance.

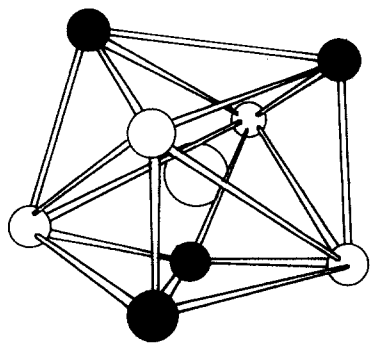

Fig. 9. CeS_8 dodecahedron with the D_{2d} symmetry.

In Fig. 8 is drawn the density of states of Ce_3S_4, computed from a Ce_6S_8 unit cell. The shaded area emphasizes the filling of bands by valence electrons up to the Fermi level e_f. The AOs we introduced bring three electrons per cerium atom and six electrons per sulfur atom, that is, 66 electrons per Ce_6S_8 unit cell. All the bands beneath −12 eV are filled with 64 electrons, then there is a gap about 2.5 eV wide. The two remaining electrons occupy the bottom of the conduction band (see Fig. 8). On the right part of Fig. 8, levels of an isolated CeS_8 dodecahedron (drawn in Fig. 9) encountered in Ce_3S_4 are shown. These levels have mainly a cerium d character. The assumed symmetry is that of a true D_{2d} dodecahedron, very similar to the slightly distorted dodecahedron actually observed.

Fig. 10 allows a careful examination of the density of states. The total density (Fig. 10(a)) is projected in Fig. 10(b) along the sulfur 3p AO (dots) and along the cerium 5d AO (dashes). One can see that the valence band (v.b.), below the gap, is essentially of S 3p character, whereas the conduction band (c.b.) is essentially of Ce 5d character. Fig. 10(c) gives the crystal orbital overlap population of the Ce–S bond as a function of energy. It shows that the electrons below the gap contribute positively to Ce–S bonding. The integrated overlap populations are 0.081 and 0.283 at the bottom and top of the v.b., respectively, proving the existence of a strong Ce–S bond. For the same bond, but above the gap, the electrons are antibonding, leading to an integrated overlap population value of 0.279 at e_f. At e_f, corresponding values for other potential bonds are −0.034 and −0.010 for S–S at 3.214 Å and S–S at 3.735 Å, respectively, showing that there is no significant sulfur–sulfur bonding, in agreement with van der Waals radii values. A positive value of 0.035 for Ce–Ce at 4.034 Å is indicative of a weak cerium–cerium bonding in this solid. The strong interaction between the AOs, revealed in partial densities of states and overlap population patterns, is in excellent agreement with the metallic behavior of the phase.

7.2. $Ce_{3-x}S_4$ $(0 \le x \le 1/3)$ and γ-$[Na]Ce_2S_3$ compounds

From the results in the previous sections, a first electronic interpretation of the properties of the $Ce_{3-x}S_4$ phases can be given. The elimination of some cerium atoms (and thence the appearance of vacancies) results in a decrease in the number of high-energy antibonding electrons. Getting rid of all the c.b. electrons implies the removal of two electrons for the Ce_6S_8 cell. Since each cerium atom is carrying three electrons, this means a withdrawal of one cerium atom out of nine, hence resulting in the formulation $Ce_{6\times 8/9}S_8$, i.e. Ce_2S_3.

One should mention that this purely electronic rigid band argument neglects any cost imputable to the breaking of eight Ce–S bonds whenever one vacancy appears, and also the effect of these vacancies on the electronic structure. In addition, a random distribution of vacancies can produce, even before the disappearance of one cerium atom out of the nine initial atoms, an

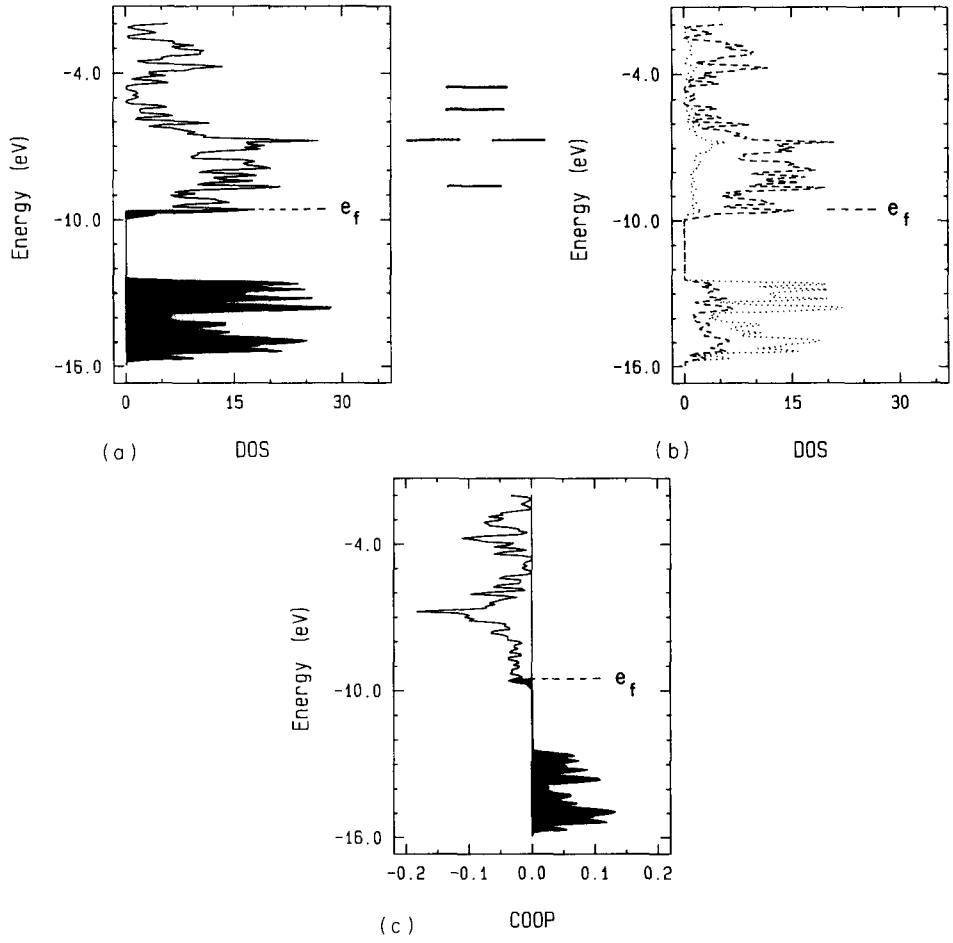

Fig. 10. (a) Total Ce_3S_4 density of states (upon 20k mesh points of the asymmetric part of the first Brillouin zone). (b) Partial sulfur p (dots) and cerium d (dashes) density of states. (c) Crystal orbital overlap population of the Ce–S bond.

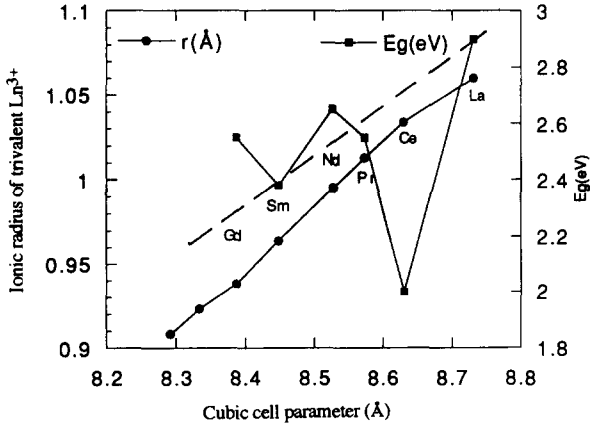

Fig. 11. Variation of the M^{3+} ions radius and of the absorption edge E_g as a function of the γ-M_2S_3 phase cell parameter [16].

Anderson transition, yielding an insulating behavior for $x < 1/3$ [15].

In this framework, the sodium atoms which replace the cerium atoms in the vacant sites would recreate bonding with the sulfur atoms. This would thus bring electrostatic stabilization while decreasing the number of electrons compared with the cerium ions. To reach the same total number of electrons as in Ce_2S_3, one should substitute in Ce_3S_4 one cerium atom out of six, giving the limit formulation $NaCe_5S_8$, i.e. $Na_{1.5}Ce_{7.5}S_{12}$ actually observed. As in the vacancy case, a random distribution of Na can generate an Anderson transition.

To model the effect of the vacancies, we calculated the density of states of the Ce_5S_8 and Ce_4S_8 cells, arbitrarily choosing the position of one and two vacancies, respectively, in the primitive cell. The major effect is a shift of the same amount of the v.b. and of

Table 9
XPS assignment (eV) of the v.b. of the γ-M_2S_3 phases (after Kaciulis et al. [17])

γ-M_2S_3	S 3p	M 4f	S 3s	M $5p_{3/2}$	M $5p_{1/2}$
La_2S_3	4.8		13.6	18.9	20.9
Ce_2S_3	5.3	2.5	13.3	19.6	22.6
Nd_2S_3	5.6	5.6	14.5	20.6	24.3
Sm_2S_3	5.7	8	14.8	22.0	26.0
Gd_2S_3	5.8	9.5		23.0	27.0
Dy_2S_3	5.8	10	14.5	24.5	29.9

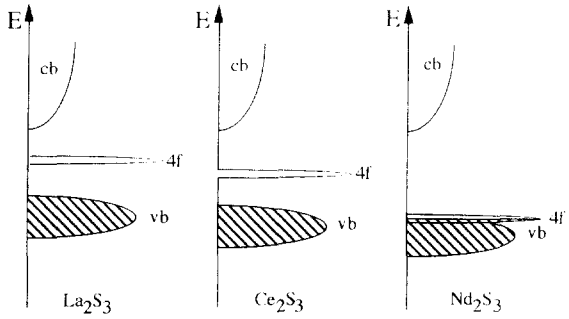

Fig. 12. Model of optical transitions in some M_2S_3 phases (see text for explanation).

the c.b. towards higher energies, resulting in an unchanged gap value. Therefore, the electronic structure is hardly changed by the occurrence of vacancies and it remains isotropic in the solid.

7.3. Structure versus color

The evolution of the M_2S_3 phases cubic cell parameters as a function of the trivalent ions radius is regular (Fig. 11). However, it is not correlated with the energy of the optical absorption edge E_g, the cerium and gadolinium phases showing a special behavior. Furthermore, since the observed color of La_2S_3 (yellow ($E_g = 2.9$ eV)) Pr_2S_3 (green ($E_g = 2.6$ eV)) and Nd_2S_3 (light green ($E_g = 2.4$ eV)) are similar, it can be infered that they originate from a v.b. to c.b. transition. For Ce_2S_3 (red ($E_g = 2.0$ eV)), transitions implying the 4f levels have to be considered.

The X-ray photoelectron spectroscopic (XPS) study of Kaciulis et al. [17] of the γ-M_2S_3 phases showed that for Ce_2S_3, the 4f levels are above that of the 3p band and the Ce_2S_3 red color is to be attributed to a 4f → c.b. transition (see Table 9). For the neodymium compound, the 4f levels would be near the top of the sulfur 3p band, leading to a green–yellow color, and a v.b. → c.b. and/or 4f → c.b. mechanism. For the other M_2S_3 phases, one has to take into account the various possible transitions between the f terms. These transition energies are in the visible light range. This model is schematically summarized in Fig. 12.

Acknowledgments

The authors thank E. Canadell for help with the Hückel calculations and fruitful discussions. This research was made possible by a grant (No. 80-02815-00) from Rhône-Poulenc (France).

References

[1] G. Velleret and J.-M. Tourre, *Proceedings of ANTEC93, New Orleans*, Society of Plastic Engineering, 1993.
[2] A.A. Kamarzin, K.E. Mironov, V.V. Sokolov, Yu.N. Malovitsky and I.G. Vasil'yeva, *J. Cryst. Growth, 52* (1981) 619.
[3] M. Evain, U-FIT Manual, *Internal Report*, IMN, Nantes, 1992.
[4] M. Evain, P. Deniard, A. Jouanneaux and R. Brec, *J. Appl. Crystallogr., 26* (1993) 563.
[5] H.M. Rietveld, *J. Appl. Crystallogr., 2* (1969) 65.
[6] C.K. Fair, *MOLEN: Structure Determination Package*, Enraf–Nonius, 1982.
[7] S.R. Hall, H.D. Flack, and J.M. Stewart (Eds.), *Xtal 3.2 Reference Manual*, Universities of Western Australia, Geneva and Maryland, 1992.
[8] G.M. Sheldrick, *Shelxtl Plus 4.0*, Siemens Analytical X-Ray Instruments, Madison, WI, 1990.
[9] (a) M.H. Whangbo and R. Hoffmann, *J. Am. Chem. Soc., 100* (1978) 6093; (b) M.-H. Whangbo, R. Hoffmann and R.B. Woodward, *Proc. R. Soc. London, Ser. A, 366* (1979) 23.
[10] W.H. Zachariasen, *Acta Crystallogr., 2* (1950) 57.
[11] M. Picon, L. Domange, J. Flahaut, M. Guittard and M. Patrie, *Bull. Soc. Chim. Fr., 8* (1960) 221.
[12] F.L. Carter, *J. Solid State Chem., 5* (1972) 300.
[13] G. Becker, J. Feldhaus, K. Westerholt and S. Methfessel, *J. Magn. Magn. Mater., 6* (1977) 1416.
[14] M. Cutler, J.F. Leavy and R.L. Fitzpatrick, *Phys. Rev. A, 133* (1964) 1143.
[15] M. Cutler and J.F. Leavy, *Phys. Rev. A, 133* (1964) 1153.
[16] *Gmelin Handbook of Inorganic Chemistry, C7, Sulfides*, Springer, Berlin, 1983, pp. 85 and 106.
[17] S. Kaciulis, A. Latisenka and A. Plesanovas, *Surf. Sci., 251/252* (1991) 330.